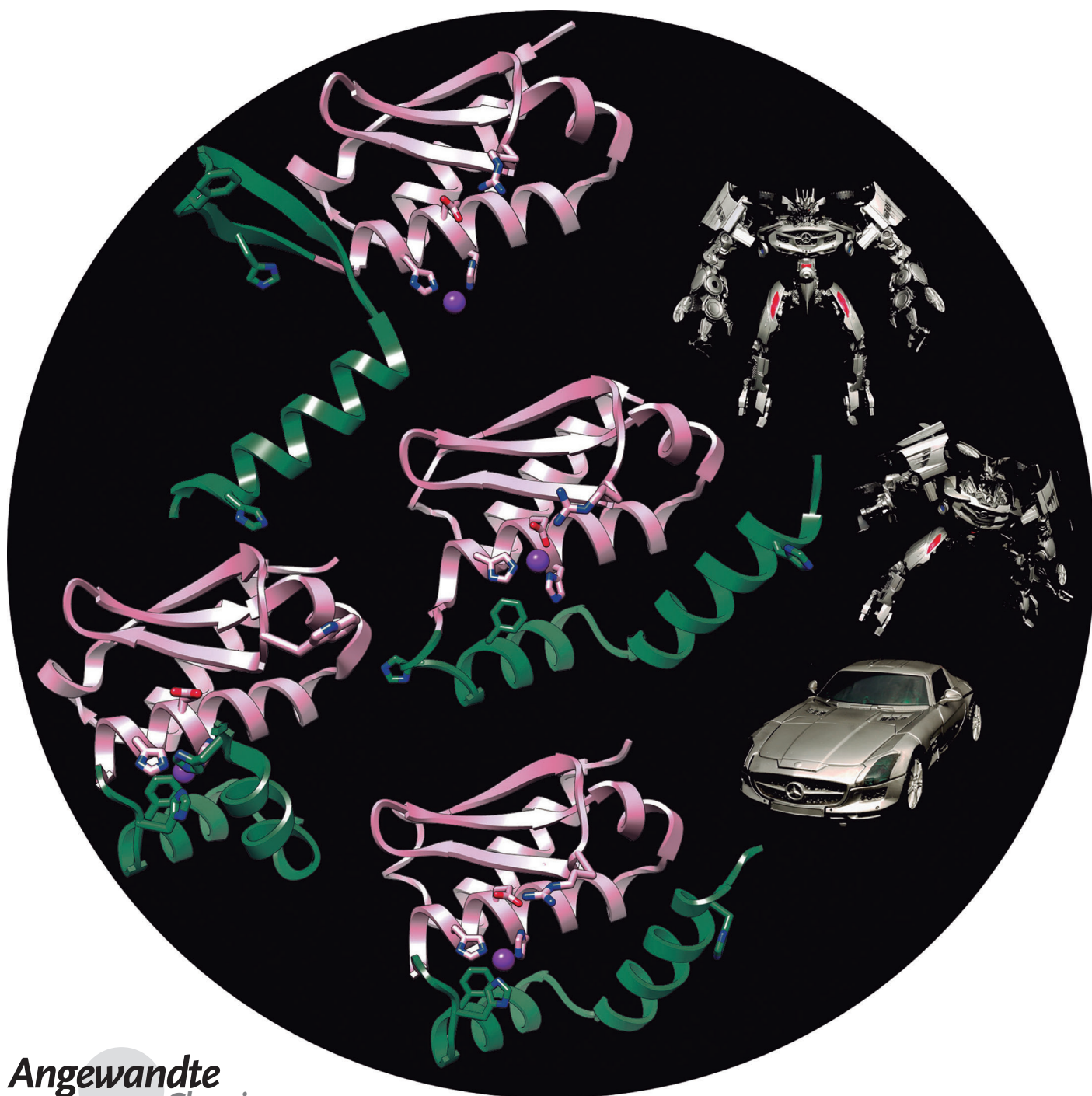


Multiple Stable Conformations Account for Reversible Concentration-Dependent Oligomerization and Autoinhibition of a Metamorphic Metallopeptidase

Mar López-Pelegrín, Núria Cerdà-Costa, Anna Cintas-Pedrola, Fátima Herranz-Trillo, Pau Bernadó, Juan R. Peinado, Joan L. Arolas, and F. Xavier Gomis-Rüth*



Abstract: Molecular plasticity controls enzymatic activity: the native fold of a protein in a given environment is normally unique and at a global free-energy minimum. Some proteins, however, spontaneously undergo substantial fold switching to reversibly transit between defined conformers, the “metamorphic” proteins. Here, we present a minimal metamorphic, selective, and specific caseinolytic metalloproteinase, *selecse*, which reversibly transits between several different states of defined three-dimensional structure, which are associated with loss of enzymatic activity due to autoinhibition. The latter is triggered by sequestering the competent conformation in incompetent but structured dimers, tetramers, and octamers. This system, which is compatible with a discrete multifunnel energy landscape, affords a switch that provides a reversible mechanism of control of catalytic activity unique in nature.

In general, the native fold of a protein in a given environment is unique and at a global free-energy minimum.^[1] However, some proteins spontaneously undergo substantial fold switching and reversibly transit between several conformers: “metamorphic” proteins.^[2] Identifying and examining such proteins is a challenge because they are highly dynamic and impossible to identify a priori.^[3] In contrast, minor rearrangement often occurs in single-domain enzymes upon binding of substrates, as shown for proteolytic enzymes of the metalloproteinase (MP) class.^[4] As to enzymatic activity, an increase in enzyme concentration usually increases activity, as more substrate can be bound and turned over.^[5] Here we describe a metamorphic minimal selective and specific caseinolytic metalloproteinase, *selecse*, which shows a reversible and concentration-dependent equilibrium between different discrete states and an associated loss of enzymatic activity due to autoinhibition.

We recently discovered a family of soluble minimal MPs named minigluzincins and characterized two of them, proabylysin and projannalysin, but we only isolated them as inactive zymogens, each in a single conformation.^[6] In the present study, we introduce *selecse* from *Methanocaldococcus jannaschii* as a novel family member. We recombinantly produced and purified *selecse* (see the Experimental Proce-

dures [EP] and Supplemental Results and Discussion [SRD] in the Supporting Information for details). In contrast to the other minigluzincins, the 110-residue full-length *selecse* corresponded to a mature, fully active MP with narrow and selective—hitherto unreported—substrate specificity that cleaved bovine milk casein at a single site on its α_{s1} chain (Suppl. Figure 1 and Suppl. Tables 1 and 2).

Selecse was extremely soluble in aqueous buffer and did not precipitate at 130 mg mL⁻¹. Thus, we studied the concentration-dependent enzymatic activity of *selecse* on a peptide that mimics the casein cleavage site (peptide CCS). Normally, peptide-bond hydrolysis by MPs is an ordered single-displacement reaction that follows simple Michaelis–Menten kinetics.^[7] This entails that higher enzyme concentrations enhance the initial rate of reaction in the pre-steady state following a hyperbolic curve until a plateau is reached upon saturation.^[5] This is found for example, with tobacco-etch virus proteinase, which is widely used in biotechnology (Figure 1 a).


Surprisingly, although *selecse* activity did indeed increase with concentration between 0.025–0.25 mg mL⁻¹, it fell sharply thereafter to become only residual at 50 mg mL⁻¹. Most interestingly, this inactive concentrated *selecse* regained maximal activity following simple dilution with buffer. Accordingly, *selecse* showed reversible enzymatic autoinhibition due to changes in concentration—and not to inhibition by the substrate or any other reagent. This, to our knowledge, is novel for peptidases.

Subsequently, we explored the oligomerization of *selecse* in solution in the concentration range 0.15–65 mg mL⁻¹ using several biophysical techniques (see EP and SRD for full details). Briefly, calibrated size-exclusion chromatography (SEC) revealed monomers, dimers, tetramers, and octamers in variable amounts depending on the concentration (Suppl. Figure 2 a). SEC-MALLS, which combines SEC with multi-angle laser light scattering (MALLS), revealed two average populations with molecular weights of 25 KDa and 80 KDa, possibly corresponding to dimeric and octameric *selecse*, respectively, along with additional species such as monomers and tetramers (Figure 1 b and Suppl. Figure 2 b). Sedimentation velocity analytical ultracentrifugation revealed the concentration-dependent presence of four oligomeric species, which would be consistent with monomers, dimers, tetramers, and octamers. This was backed by equilibrium velocity experiments showing concentration-dependent average masses ranging between monomers + dimers and octamers (Figure 1 c and Suppl. Table 3). Chemical crosslinking experiments followed by SDS-PAGE, in turn, showed monomers, dimers, monomer–dimer complexes, and tetramers. Higher oligomerization species were not detected due to intrinsic experimental limitations (Suppl. Figure 2 c). The circular dichroism spectra of *selecse*, with either zinc or nickel in the catalytic site, displayed the typical shape of well-folded mostly α -helical proteins (Suppl. Figure 2 d). Finally, SAXS revealed that the protein did not aggregate at concentrations of up to 65 mg mL⁻¹ (Suppl. Table 4, Figure 1 d, Suppl. Figures 3 and 4). These results further showed that the relative population of the oligomeric species in solution was concentration dependent. In addition, single-value decomposition analysis of the SAXS dataset indicated that four

[*] M. López-Peigrín,^[†] Dr. N. Cerdà-Costa,^[†] Dr. A. Cintas-Pedrola, Dr. J. R. Peinado,^[§] Dr. J. L. Arolas, Prof. Dr. F. X. Gomis-Rüth
Proteolysis Lab, Molecular Biology Institute of Barcelona
CSIC, Barcelona Science Park
c/Baldiri Reixac, 15–21, 08028 Barcelona (Spain)
E-mail: fxgr@ibmb.csic.es
Homepage: <http://www.ibmb.csic.es/home/xgomis>
F. Herranz-Trillo, Dr. P. Bernadó
Centre de Biochimie Structurale, INSERM U1054
CNRS UMR 5048, Université Montpellier 1 and 2
29 rue de Navacelles, 34090 Montpellier (France)

[§] Present address: Department of Medical Sciences
University of Castilla-La Mancha, 13071 Ciudad Real (Spain)

[†] These authors contributed equally to this work.

 Supporting information for this article (including experimental procedures, supplemental results and discussion, acknowledgments, supplemental references, tables, figures, and movies) is available on the WWW under <http://dx.doi.org/10.1002/anie.201405727>.

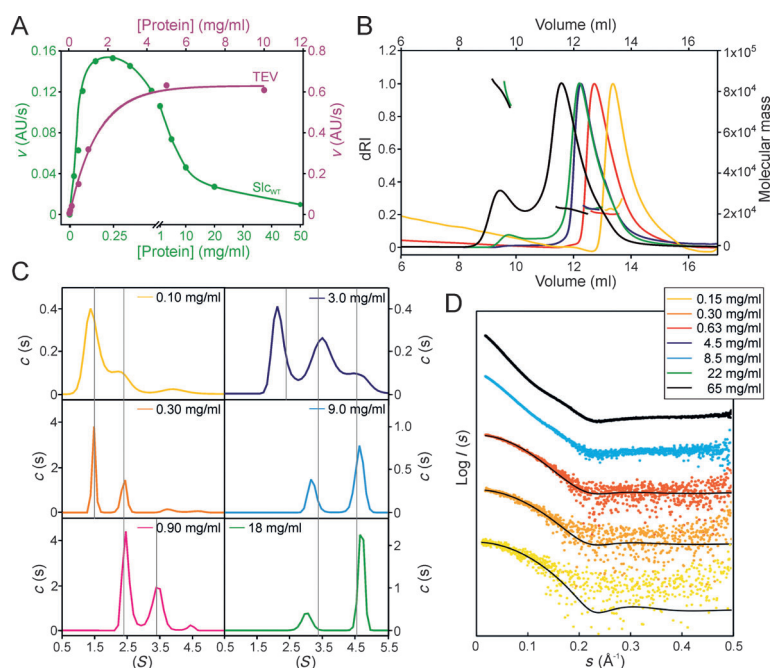


Figure 1. A polyoligomeric metallocaseinase with abnormal activity. A) Proteolytic activity of wild-type secase on peptide CCS (green curve). Tobacco-etch virus proteinase mutant S219V, which shows comparable catalytic efficiency to secase but normal concentration-dependent activity, is shown for comparison (purple curve). B) SEC-MALLS of secase at selected initial concentrations (0.15–65 mg mL⁻¹; see also Suppl. Figure 2b). The peak pattern moves towards smaller elution volumes with increasing protein concentration, thus suggesting protein oligomerization. Curves are colored according to the inset in panel (D). dRI = differential refracting index. C) Analytical ultracentrifugation curves at six selected concentrations depicting the concentration-dependent oligomeric populations. Essentially, monomers are predominantly found at 0–0.3 mg mL⁻¹; dimers at 0.3–2 mg mL⁻¹; tetramers at 2–6 mg mL⁻¹; and octamers at > 6 mg mL⁻¹. *S* = sedimentation coefficient, *c*(*S*) = continuous sedimentation coefficient distribution. D) SAXS intensity profiles, *I*(*s*), as a function of the momentum transfer, *s*, measured for wild-type secase at selected concentrations (see Suppl. Figure 3 for all curves). Profiles have been displaced along the *I*(*s*) axis for comparison. The experimental scattering curves at the three lowest concentrations studied indicate a mixed population of monomers and dimers based on the crystallographic structures of slc₁ and slc₂ (black curves).

species (monomers, dimers, tetramers, and octamers) were present.

Summarizing, biophysical analyses in solution indicated the presence of mixtures of monomers, dimers, tetramers, and octamers, with higher concentrations leading to greater oligomerization but not indiscriminate aggregation or precipitation. The concentrations at which monomeric secase was predominant coincided with those of maximal enzymatic activity (0.2–0.3 mg mL⁻¹; Figure 1a), thus indicating that the monomer is the active species and that oligomers correspond to self-inhibiting species in all cases (see below). This would explain why higher enzyme concentrations yielded lower activity (Figure 1a) and is reminiscent of previous reports on oligomerization inhibiting the activity of phospholipase A2.^[9] Notably, simple dilution with buffer reversed oligomerization to yield monomers and restore activity.

To identify the molecular determinants of this behavior, we crystallized and solved the structure of wild-type secase

(see EP, SRD, and Suppl. Table 5). We obtained three crystal forms—orthorhombic, tetragonal, and hexagonal—which serendipitously corresponded to monomeric (slc₁), dimeric (slc₂), and tetrameric (slc₄) forms of secase, respectively. This indicated that at least three of the oligomerization states found in solution had a counterpart in the form of a stable, isolatable species, each one favored by particular crystallization conditions. The crystal structure of monomeric slc₁ reveals—by comparison with several functional but otherwise unrelated MPs—that the overall architecture, the metal-binding site, and the active-site environment are consistent with a competent and functional mature enzyme (see Refs. [7b,10]). This conclusion is supported by the enzymatic activity found for secase in solution associated with a monomeric species (see above). It is also reinforced by SAXS for which the experimental scattering curves at the three lowest concentrations—covering the activity maximum of the enzyme—clearly indicated mixed populations of monomers and dimers based on the crystallographic coordinates of slc₁ and slc₂ (see below), with the monomeric fraction at the two lowest concentrations reaching 70% (see Figure 1d, SRD, and Suppl. Figures 3 and 4).

At 13.1 kDa, slc₁ is the smallest active peptidase structurally characterized to date and it has a compact globular shape 35–40 Å in diameter (Figure 2a). It consists of an upper N-terminal subdomain (NTS; residues M¹–Y⁷⁶) and a lower C-terminal subdomain (CTS; G⁷⁷–K¹⁰⁹), which are connected by a mostly hydrophobic interface (Suppl. Table 6) and separated by a horizontal central active-site cleft (Figure 2b). The NTS is an α/β-sandwich, with a three-stranded mixed β-sheet (β1–β3; Suppl. Table 7) that forms the roof of the secase moiety (Figure 2a). Two roughly parallel α-helices (“backing helix” α1 and “active-site helix” α2) are attached to the convex surface of the sheet, which faces the central core of the protein. A short helical segment (“linking helix” αB) is inserted in the loop connecting strand β3 with helix α2 (Lβ3α2). Helix α2 roughly parallels the active-site cleft and ends with the last residue of the NTS at Y⁷⁶. It encompasses a metal-binding motif, H⁶⁹–E⁷⁰–X–X–H⁷³, which is characteristic of MPs and includes two metal-binding histidines and a general base/acid glutamate essential for catalysis.^[11] Residue H⁸⁰, imbedded within Lα2α3 of the CTS, is the third metal ligand. The CTS mainly consists of two helices (“glutamate helix” α3 and “C-terminal helix” α4), whose axes intersect at roughly 90°. Helix α3 contains F⁸⁴ at the center of the “Ser/Gly-turn”,^[6,11a] which creates a hydrophobic base for the metal-binding site and contributes to its stabilization. The active-site cleft of secase is framed by helix α2; the “upper-rim” strand β2 of the NTS sheet and the preceding “bulge-edge segment” (L³⁴–I³⁸); helices α3 and α4; and Lα2α3, in particular through the side chains of K⁷⁸ and Y⁷⁹. The catalytic metal ion resides at the bottom left of

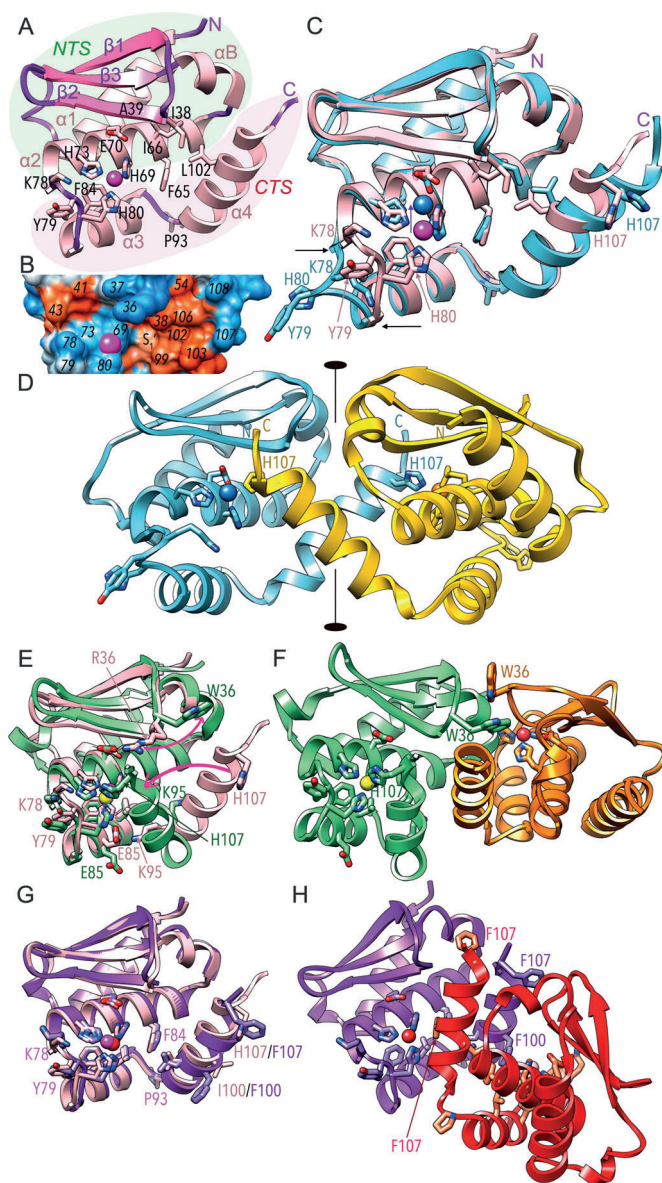


Figure 2. Competent monomer versus incompetent dimers. A) Ribbon representation of slc_1 in standard orientation.^[8] Helices ($\alpha 1$, αB , and $\alpha 2$ – $\alpha 4$) are shown in pink, β -strands ($\beta 1$ – $\beta 3$) in magenta, and loops/coils in purple. For extent and nomenclature of regular secondary structure elements, see Suppl. Table 7. Selected residues are shown for their side chains, as is the catalytic metal ion (magenta sphere). The NTS and the CTS are shown over light green and light purple background, respectively. B) Surface representation of slc_1 colored according to Kyte–Doolittle hydrophobicity (blue = hydrophilic over white to orange = hydrophobic) in the same orientation as in (A) showing the active-site cleft with the hydrophobic S_1' specificity pocket. C) Superposition of slc_1 (in pink) and the slc_2 monomer (in cyan). Depicted are the respective metal ions, which are shifted relative to each other (purple arrow). Horizontal black arrows pinpoint the anchor points around which the conformational rearrangement occurs. D) Overall structure of symmetric dimeric slc_2 (chains in cyan and gold) depicted so that the crystallographic dyad (black horizontal ellipses joined by a line) is in the plane of the picture. E) Superposition of slc_1 (in pink) and molecule B of the $R^{36}W$ seletase dimeric mutant (slc_2 ; in light green). Magenta arrows pinpoint the side-chain movement at position 36 owing to the mutation and the 50° rotation of C-terminal helix $\alpha 4$. F) Structure of the asymmetric dimer of slc_2 consisting of helix-rotated molecule B (green) and close-to-native molecule A (orange). Both active-site clefts are blocked but following different mechanisms. Note the two W^{36} side chains at the interface. G) Superposition of slc_1 (in pink) and one of the two equivalent close-to-native monomers of seletase $I^{100}F + H^{107}F$ dimeric mutant (slc_2 ; in purple). H) Inactive dimer of slc_2 (in purple and red).

the cleft (Figure 2a,b). At its right, a deep hydrophobic S_1' pocket is shaped by I^{38} , A^{39} , F^{65} , I^{66} , L^{102} , and the solvent-accessible ring surface of H^{69} . This pocket optimally accommodates a phenylalanine in the P_1' position of substrates as found at the casein cleavage site. The slc_1 moiety is held together by a central hydrophobic core, which traverses the entire molecule, and several of the contributing residues also shape the NTS–CTS interface (Figure 2a and Suppl. Table 6).

The crystal structure of slc_2 shows a dimer (Suppl. Table 8), and superposition of slc_1 and slc_2 monomers reveals good overall fit, with only minor differences within the NTS (see Figure 2c). However, major metamorphic rearrangement is observed around the metal-binding site (see Figure 2c and Suppl. Movie 1). In slc_2 , at the beginning of CTS, $La2\alpha 3$ folds outward between G^{77} and I^{81} , with a maximal displacement of 7 Å. This causes the third metal-binding protein residue in slc_1 , H^{80} , to swing out and protrude from the molecular surface. This, in turn, leads to an upward shift of the

catalytic metal towards the general base/acid E^{70} (Figure 2c). Two seletase monomers associate through C_2 symmetry under occlusion of a large surface (2130 \AA^2 ; see Suppl. Table 8 and Figure 2d) and so the third metal-binding site is taken over by H^{107} from helix $\alpha 4$ of the symmetric molecule. Accordingly, this H^{80}/H^{107} ligand swap is an intermolecular event that yields a catalytically incompetent metal-binding site and a blocked active-site cleft in slc_2 . This is consistent with oligomerization coinciding with inactive species in solution (see above).

As in slc_2 , the protomer of tetrameric slc_4 shows good overall fit with slc_1 within the NTS, including the position and conformation of most side chains at the NTS–CTS interface. However, both major displacement and drastic conformational rearrangement are observed in the CTS (see Figure 3a and Suppl. Movie 2). The segment of the active-site helix with the first two metal ligands undergoes slight displacement (Figure 3a). Downstream loop $La2\alpha 3$ and glutamate helix $\alpha 3$ —which is virtually unchanged in both slc_1 and slc_2 —unfold and give rise to strands $\beta 4$ and $\beta 5$, which adopt a canonical β -ribbon structure (Figure 3a and Suppl. Table 7). Such long stretches of a protein only rarely undergo such dramatic transitions.^[12] The β -ribbon protrudes away from the molecular moiety (Figure 3a,b), as a result of which metal-ligand H^{80} shifts roughly 16 Å from its position in slc_1 and no longer binds the metal. In contrast with $\alpha 3$, the C-terminal helix $\alpha 4$ keeps its helical structure but is displaced about 30 Å apart on average in slc_4 (Figure 3a). Overall, this metamorphic structural transition of seletase is stabilized by the association of four monomers in the crystal (Figure 3b–d, Suppl. Table 8, and Suppl. Movie 2), which would explain tetrameric oligomerization in solution (see above). The oligomer is a compact, almost spherical self-inhibitory particle 60–75 Å in diameter

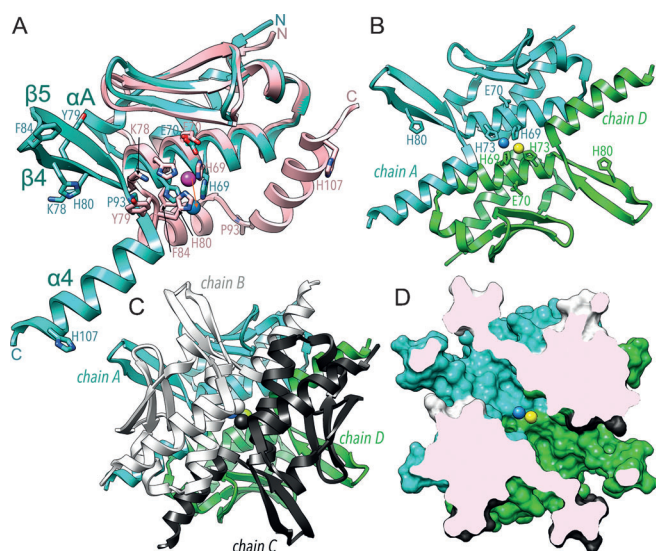


Figure 3. A compact autoinhibitory tetrameric particle. A) Superposition of slc_1 and slc_4 monomers in pink (magenta metal ion) and turquoise (blue metal ion), respectively, in the view of Figure 2a. Only the distinct secondary structure elements of slc_4 are labeled (see also Suppl. Table 7). Relevant residues undergoing major rearrangement are displayed for both structures and labeled. The metal is shifted downwards (red arrow). B) Within the slc_4 tetramer, two neighbor monomers as in (A), in turquoise (chain A; metal in blue) and light green (chain D; metal in yellow), bind over a crystallographic dyad perpendicular to the plane of the picture. This gives rise to a nonfunctional dimetallic zinc site bound by H⁶⁹ and H⁷³ of either monomer. C) Two dimers as in (B), in turquoise/light green (chains A and D) and white/dark gray (chains B and C), associate face to face under a relative 90° rotation to yield the overall tetrameric particle, with two dimetallic zinc sites in the particle lumen. D) Surface representation of (C) after clipping off the frontal part to delineate the central particle channel. Only the dimetallic site depicted in (B) is shown for clarity.

(Figure 3c,d). One monomer (chain A) interacts through D_2 symmetry—by hiding a total interface of 9850 Å²—with two neighboring molecules (chains B and D) through mixed hydrophobic/hydrophilic contacts, and with one opposite monomer (chain C) through hydrophobic contacts (Suppl. Table 8). Two large elliptical openings (minor axis \approx 16 Å, major axis \approx 21 Å; Figure 3d and Suppl. Movie 2) on opposite faces of the particle are framed by upper-rim strands β_2 and $L\beta_5\alpha_4$ of two vicinal monomers (AB and CD). Access to the particle lumen through these entrances is limited by the respective β -ribbons, which protrude away from the particle surface and do not contact each other. The central lumen of the particle features a channel 50 Å in length and 15 Å in diameter and allocates two internal dimetallic zinc-binding sites. Each of them results from the fusion of two neighboring metal sites as originally found in slc_1 (chains AD and BC, respectively), with the two metal ions of each site roughly 3 Å apart (Figure 3b,d). Overall, this new conformation radically alters the structural segments that shape the S_1' pocket and the active-site cleft in competent slc_1 and, thus, indicates that, like slc_2 , the tetrameric slc_4 structure corresponds to an inactive species. This, again, is consistent with tetramers coinciding with inactive species in solution.

Given the importance of the C-terminal helix α_4 and loop $L\beta_1\beta_2$ in oligomerization, we selected residues R³⁶, I¹⁰⁰, I¹⁰³, and H¹⁰⁷, which had been observed to participate in dimerization in slc_2 and tetramerization in slc_4 (Suppl. Table 8), and generated a total of seven single, double, and triple point mutants in an attempt to ablate the interactions responsible for oligomerization and thus obtain monomeric forms. In addition, we constructed two deletion mutants targeting α_4 , lacking four ($slc\Delta C4$) and eight ($slc\Delta C8$) C-terminal residues. Moreover, we cloned two close orthologues from *Methanoterris igneus* and *Methanocaldococcus fervens*, which can be envisaged as natural fivefold and 19-fold point mutants of selease (see EP and SRD for full details). All protein variants were produced, purified, and concentrated similarly to the wild-type except for $slc\Delta C4$, which was obtained with lower yields and could only be maximally concentrated to 5.0 mg mL⁻¹, and $slc\Delta C8$, which was insoluble and was discarded. This finding pointed to a stabilizing effect of helix α_4 on the whole protein despite its overall flexibility in the various structures analyzed. Despite differences in the oligomer populations, all mutants displayed a concentration-dependent equilibrium between monomers, dimers, tetramers, and octamers and a reduction in activity as concentration increased, similar to the wild-type (Suppl. Figure 5). These results indicate that selease is highly plastic, which allows it to adapt to potentially deleterious point mutations and retain its capacity to oligomerize.

This plasticity is backed by further structural studies. Out of all the aforementioned mutants and orthologues, we managed to crystallize variants R³⁶W (hereafter slc_2) and I¹⁰⁰F + H¹⁰⁷F (hereafter slc_2') and solved their crystal structures (see Figures 2e–h and Suppl. Movie 3). Most interestingly, slc_2' showed a novel dimeric quaternary structure, distinct from slc_2 , which displayed each protomer in a different conformation despite the chemical identity of the molecules. One molecule (A) essentially displays the conformation of functional monomeric slc_1 , including the metal site and the active-site cleft. It only differs significantly from the latter at $L\beta_1\beta_2$, which, owing to the side-chain replacement at position 36, causes the entire loop and thus the latter side chain to undergo major rearrangement towards the molecular moiety. The other molecule (B) also essentially coincides with slc_1 but only until the glutamate helix. Thereafter, a 90° rotation around bond N–Ca of K⁹⁵ results in C-terminal helix α_4 being rotated as a rigid body by 50° so as to approach and thus sterically block its own active-site cleft on its primed side. This further causes H¹⁰⁷ to bind the catalytic metal, as observed in slc_2 , except that here this is an intramolecular rather than an intermolecular event (compare Figure 2d–f). This novel conformation of a selease variant in molecule B is stabilized by an asymmetric interaction between C-terminal helices with molecule A triggered by an edge-to-face interaction of the W³⁶ side chains (Figure 2f). This arrangement, in turn, causes the active-site cleft of molecule A to be blocked for substrate access by helix α_4 of molecule B, with Y⁵⁷ of the latter interacting with the S_1' pocket of molecule A. The metal-binding site of the latter, in contrast, is unaffected. Accordingly, slc_2' corresponds—like slc_2 —to an inhibited conformation.

As to slc_2 , superposition of the two essentially identical monomers in the asymmetric unit onto slc_1 revealed a conformation that was close to that of the functional wild-type monomer, except that the end of the C-terminal helix was slightly unwound and more flexible owing to the two point mutations (Figure 2g). However, the two phenylalanine residues at positions 100 and 107 make two slc_2 monomers symmetrically bind mainly through their respective C-terminal helices, which run roughly parallel to each other. As a result the nonprimed sides of the active-site clefts are occluded and the phenylalanine rings at position 100 penetrate the S_1' specificity pocket of the symmetric partner, as this residue matches the specificity of the enzyme. Further symmetric contacts are observed between the F^{107} side chain of one molecule and loop $L\beta 1\beta 2$ of the other, which enhance the overall flexibility of these regions. Accordingly, the structure of slc_2 provides yet another mechanism of inhibition of selease, in this case merely by the shielding of the cleft (Figure 2h). Thus, the two crystal structures of slc_2 and slc_2 may represent genuine dimeric conformations of the mutants triggered by the respective side-chain replacements, as none of the corresponding structures was trapped in crystals of the wild-type protein. This implies that replacement of just one and two residues leads to two new structures of selease (thus totaling five), supporting the metamorphic character of this protein.

Summarizing, we have succeeded in identifying and probing for the first time the structural transitions of a natural metamorphic protein with a multifunnel folding energy landscape. Although metamorphic proteins may be encoded by a relevant fraction of all genomes, the lack of bioinformatics and structural approaches to identify them from the sequence restricts their discovery to serendipity. Consistently, to our knowledge 3D structural evidence for their existence has only been published for two natural proteins,^[2,13] which just flip between two folds: ubiquitin protein ligase inhibitor Mad2^[14] and the chemokine lymphotactin.^[15] In selease, the energy basins are occupied by distinct fully structured and stable states and not by unfolded species or molten globules (Figure 4 and Suppl. Movies 1–3). One conformer is catalytically competent and the others are incompetent but they coexist in equilibrium. These transitions between species are triggered by major rearrangement after residue G^{77} at the NTS–CTS interface, and they mainly affect the CTS. This is consistent with each subdomain corresponding to a distinct folding unit or foldon^[16] and the subdomain interface acting as a reversible zipper. The high flexibility of CTS was further verified by computational analysis of local conformational frustration and assessment of interdomain flexibility based on the elastic network model (see SRD and Suppl. Figure 7). In addition, the thermodynamic consistency of interconversion was further backed by the calculated geometric and thermodynamic parameters of the solvation free energy of folding and of dissociation, as well as compactness, for wild-type selease structures (see SRD and Suppl. Table 8). Owing to inherent flexibility of the CTS, it avoids kinetic trapping in an irreversible misfolded state during conversion between alternate conformers through the protein–protein interactions of oligomeric species as previously suggested for metamorphic

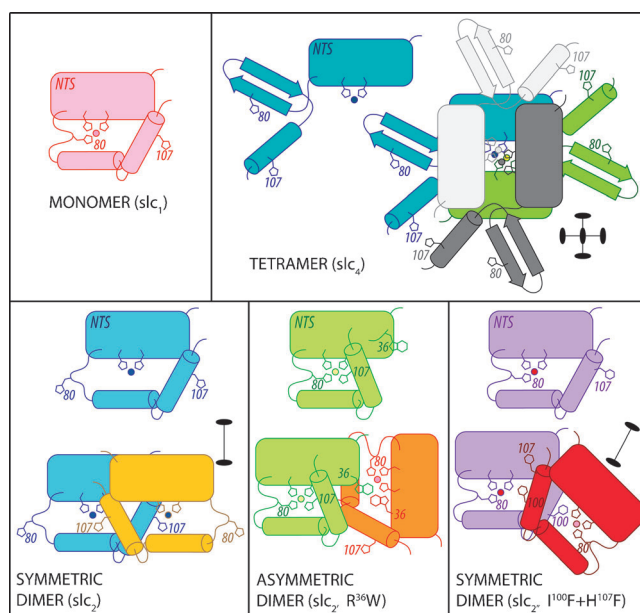


Figure 4. Scheme illustrating the topology of the distinct selease structures reported. A black ellipse stands for a dyad vertical to the plane, two black ellipses connected by a line stand for a dyad in the plane. NTS, N-terminal subdomain; histidines H^{69} , H^{73} , H^{80} , and H^{107} are shown. In slc_2 , R^{36} is replaced by tryptophan; in slc_2 , I^{100} and H^{107} are replaced by phenylalanine.

proteins.^[13] In our view, it is a striking observation that simple dilution/concentration of a sample at room temperature triggers fold switches that cause the repacking of a hydrophobic core and exposure of new binding surfaces, which in turn generate the spontaneous conversion between active monomers and inactive oligomers. This finding indicates that the energy barriers separating the minima are surmountable and that interconversion may proceed without passing through fully unfolded states,^[2] as suggested by the finding of largely conserved NTS foldons. Finally, our results also provide the first evidence for a peptidase with a reversible, strictly concentration-dependent reduction of activity at higher concentrations, which is triggered by the sequestering of the competent conformation in incompetent but structured oligomers. This system affords a switch that provides a unique and reversible mechanism of control of catalytic activity in nature.

Received: May 28, 2014

Published online: August 27, 2014

Keywords: metallopeptidases · metamorphic proteins · protein folding · protein structures

- [1] C. B. Anfinsen, *Science* **1973**, *181*, 223–230.
- [2] A. G. Murzin, *Science* **2008**, *320*, 1725–1726.
- [3] S. C. Goodchild, P. M. G. Curmi, L. J. Brown, *Biophys. Rev. Lett.* **2011**, *3*, 143–153.
- [4] P. Towler, B. Staker, S. G. Prasad, S. Menon, J. Tang, T. Parsons, D. Ryan, M. Fisher, D. Williams, N. A. Dales, M. A. Patane, M. W. Pantoliano, *J. Biol. Chem.* **2004**, *279*, 17996–18007.

- [5] V. Henri, *C. R. Hebd. Seances Acad. Sci.* **1902**, 135, 916–919.
- [6] M. López-Peigrín, N. Cerdà-Costa, F. Martínez-Jiménez, A. Cintas-Pedrola, A. Canals, J. R. Peinado, M. A. Martí-Renom, C. López-Otín, J. L. Arolas, F. X. Gomis-Rüth, *J. Biol. Chem.* **2013**, 288, 21279–21294.
- [7] a) L. Polgár in *Proteolytic enzymes—Tools and targets* (Eds.: E. E. Sterchi, W. Stöcker), Springer, Berlin, **1999**, pp. 148–166; b) B. W. Matthews, *Acc. Chem. Res.* **1988**, 21, 333–340.
- [8] F. X. Gomis-Rüth, T. O. Botelho, W. Bode, *Biochim. Biophys. Acta Proteins Proteomics* **2012**, 1824, 157–163.
- [9] a) T. L. Hazlett, E. A. Dennis, *Biochemistry* **1985**, 24, 6152–6158; b) D. H. Fremont, D. H. Anderson, I. A. Wilson, E. A. Dennis, N. H. Xuong, *Proc. Natl. Acad. Sci. USA* **1993**, 90, 342–346.
- [10] a) W. Bode, F. X. Gomis-Rüth, R. Huber, R. Zwillig, W. Stöcker, *Nature* **1992**, 358, 164–167; b) F. X. Gomis-Rüth, *J. Biol. Chem.* **2009**, 284, 15353–15357.
- [11] a) F. X. Gomis-Rüth, *Crit. Rev. Biochem. Mol. Biol.* **2008**, 43, 319–345; b) N. Cerdà-Costa, F. X. Gomis-Rüth, *Protein Sci.* **2014**, 23, 123–144.
- [12] X. Zhou, F. Alber, G. Folkers, G. H. Gonnet, G. Chelvanayagam, *Proteins Struct. Funct. Genet.* **2000**, 41, 248–256.
- [13] P. N. Bryan, J. Orban, *Curr. Opin. Struct. Biol.* **2010**, 20, 482–488.
- [14] M. Mapelli, L. Massimiliano, S. Santaguida, A. Musacchio, *Cell* **2007**, 131, 730–743.
- [15] R. L. Tuinstra, F. C. Peterson, S. Kutlesa, E. S. Elgin, M. A. Kron, B. F. Volkman, *Proc. Natl. Acad. Sci. USA* **2008**, 105, 5057–5062.
- [16] A. R. Panchenko, Z. Luthey-Schulten, P. G. Wolynes, *Proc. Natl. Acad. Sci. USA* **1996**, 93, 2008–2013.